

Determination of the subcellular localization and mechanism of action of ferrostatins in suppressing ferroptosis

Michael M. Gaschler, Fanghao Hu, Huizhong Feng, Andreas Linkermann, Wei Min, and Brent R. Stockwell

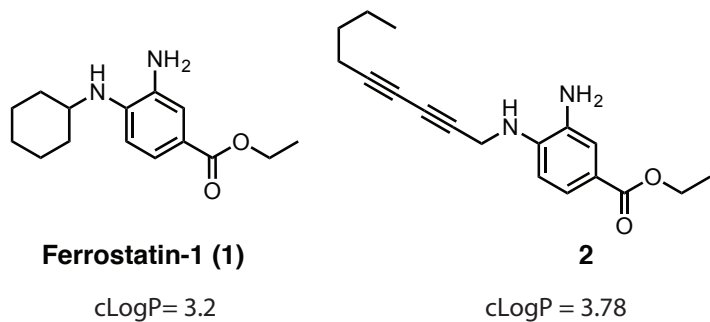
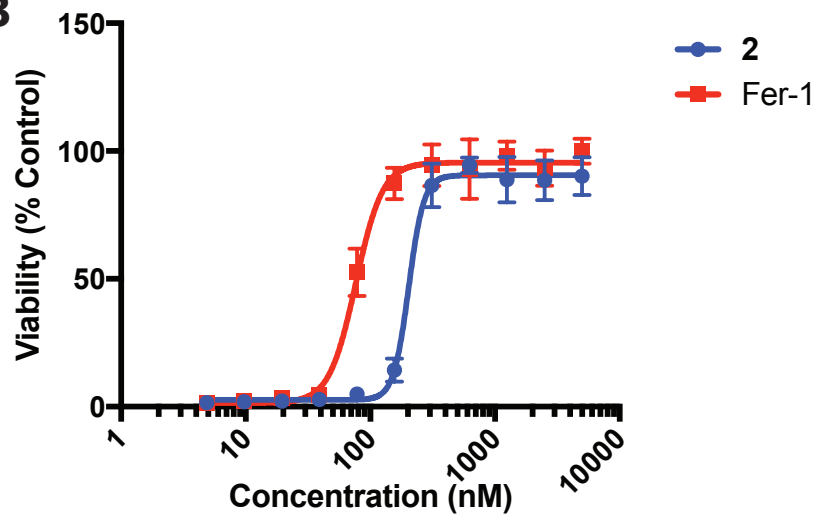
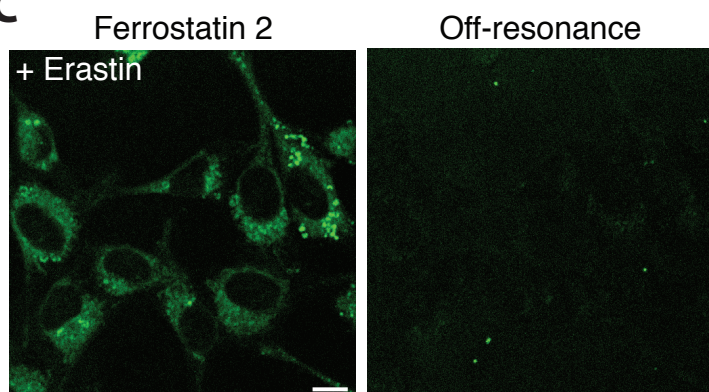
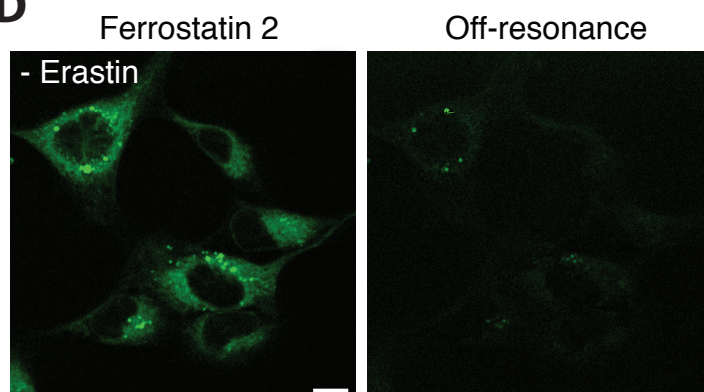
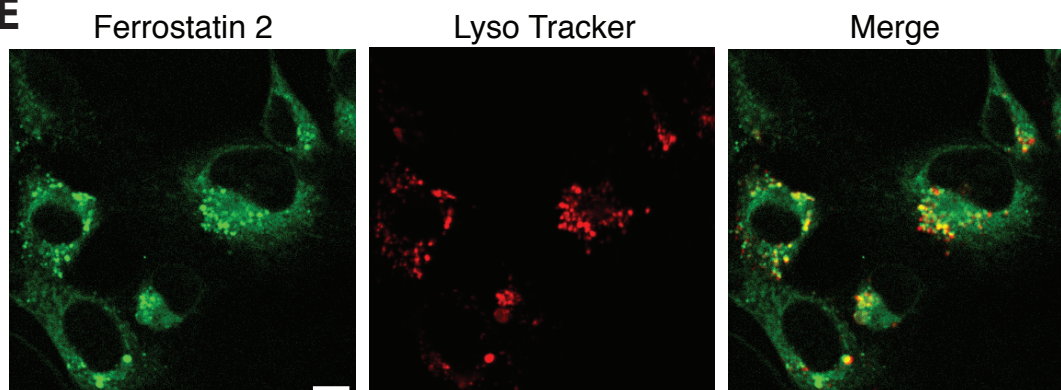
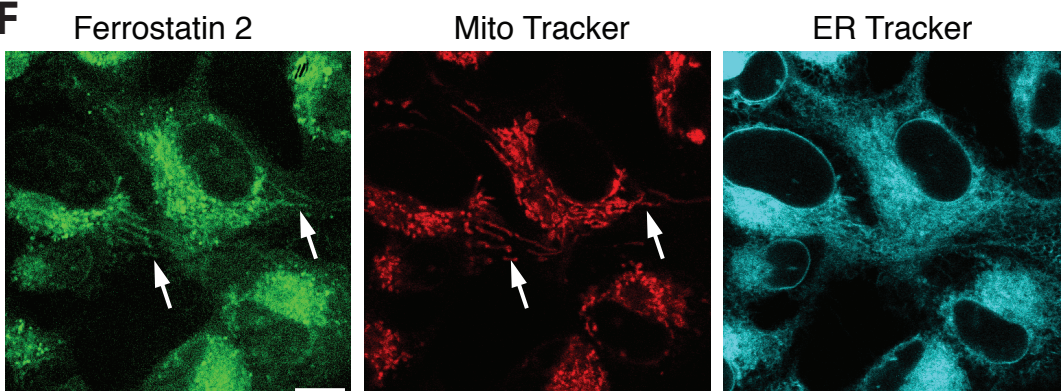
ACS Chem. Biol., **Just Accepted Manuscript** • DOI: 10.1021/acscchembio.8b00199 • Publication Date (Web): 07 Mar 2018

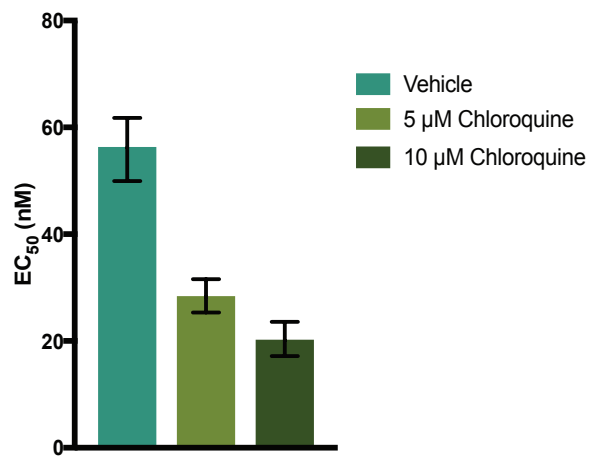
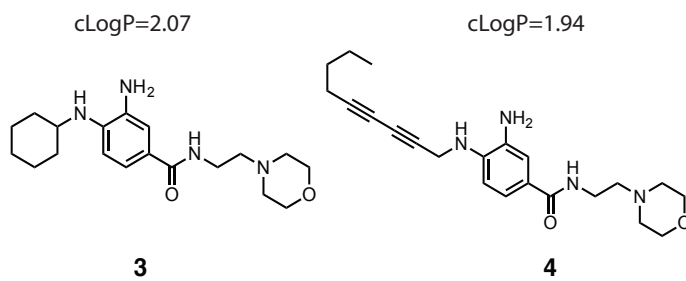
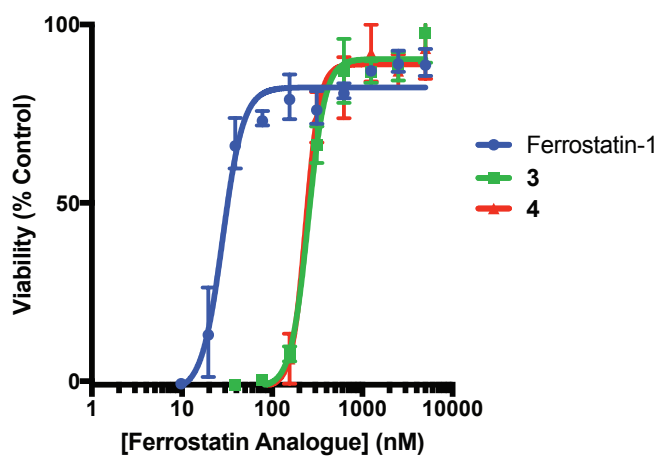
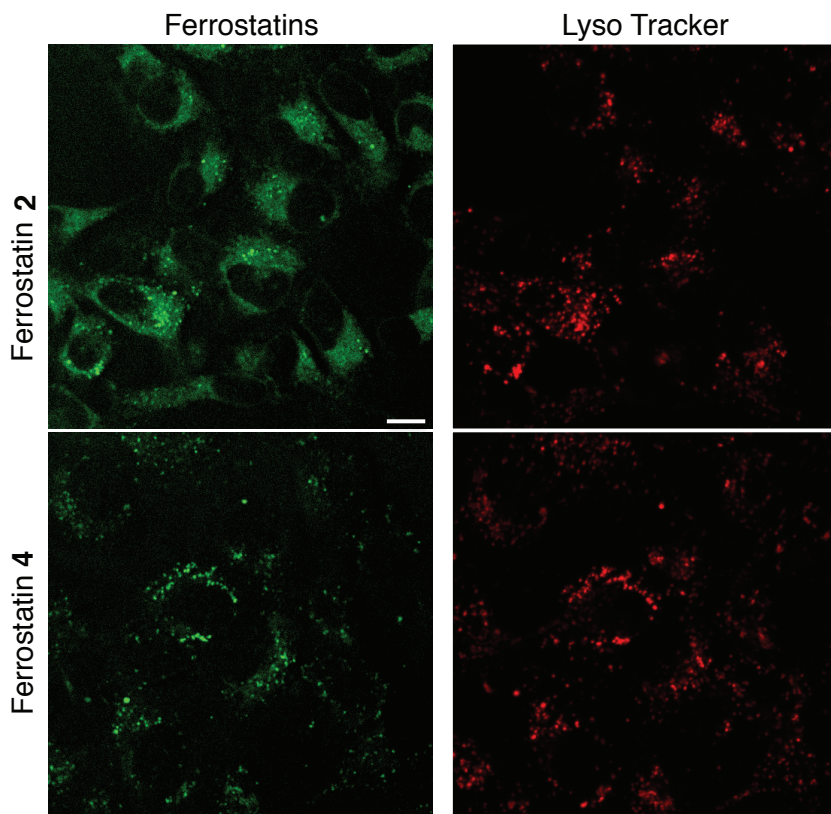
Downloaded from <http://pubs.acs.org> on March 8, 2018

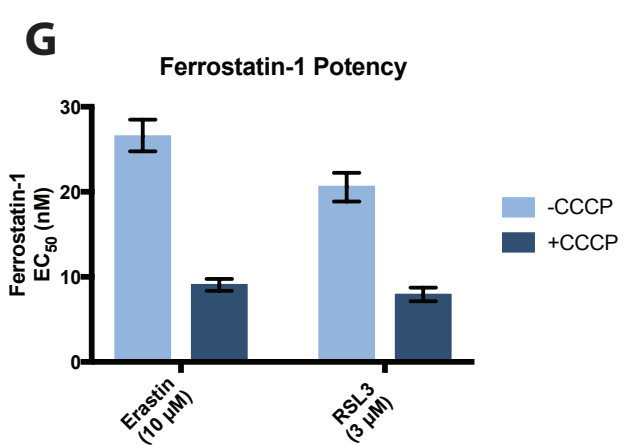
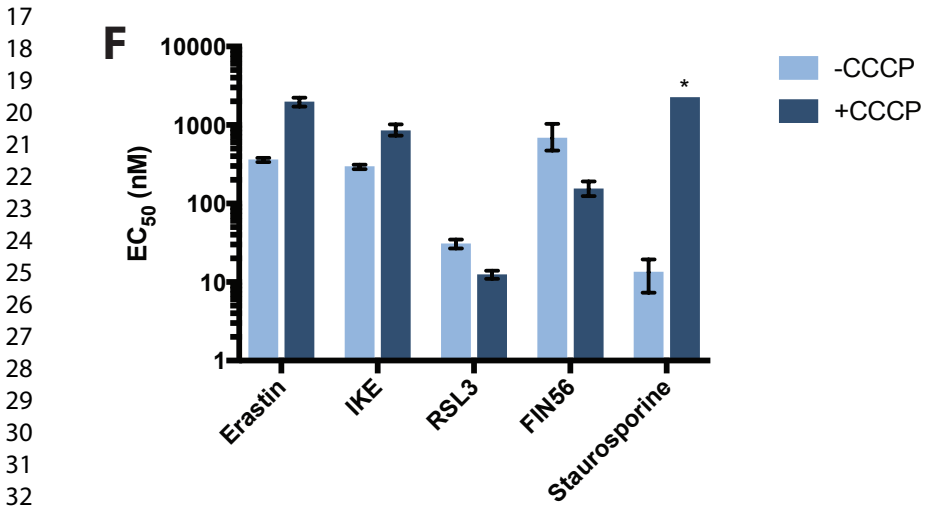
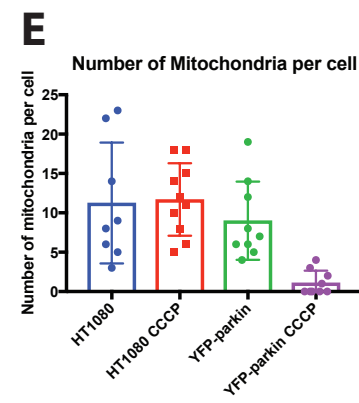
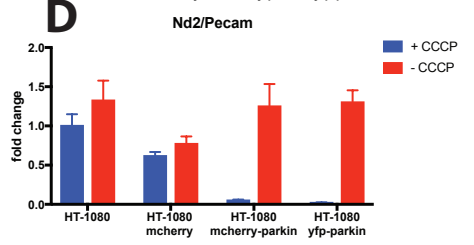
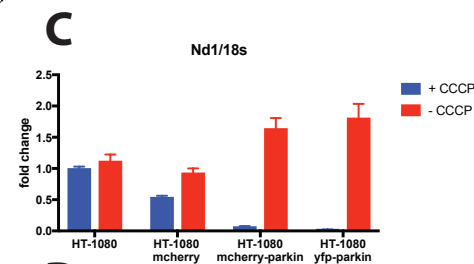
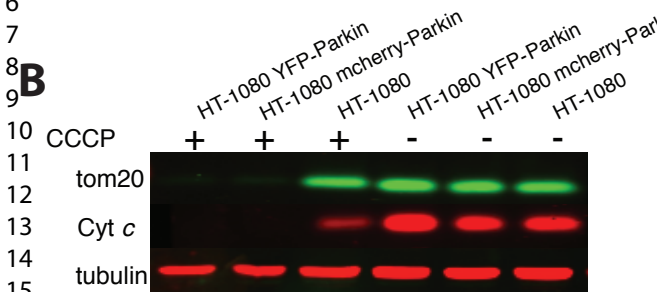
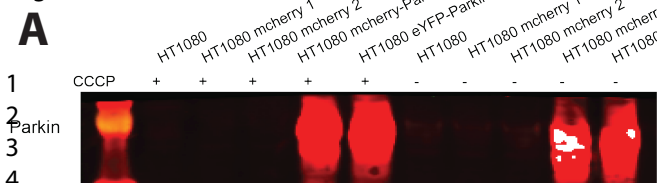
Just Accepted

“Just Accepted” manuscripts have been peer-reviewed and accepted for publication. They are posted online prior to technical editing, formatting for publication and author proofing. The American Chemical Society provides “Just Accepted” as a service to the research community to expedite the dissemination of scientific material as soon as possible after acceptance. “Just Accepted” manuscripts appear in full in PDF format accompanied by an HTML abstract. “Just Accepted” manuscripts have been fully peer reviewed, but should not be considered the official version of record. They are citable by the Digital Object Identifier (DOI®). “Just Accepted” is an optional service offered to authors. Therefore, the “Just Accepted” Web site may not include all articles that will be published in the journal. After a manuscript is technically edited and formatted, it will be removed from the “Just Accepted” Web site and published as an ASAP article. Note that technical editing may introduce minor changes to the manuscript text and/or graphics which could affect content, and all legal disclaimers and ethical guidelines that apply to the journal pertain. ACS cannot be held responsible for errors or consequences arising from the use of information contained in these “Just Accepted” manuscripts.

Potency of Ferrostatin Rescue

A**B****C****D****E****F**

A Ferrostatin-1 Potency
With Chloroquine Addition**B** ACS Chemical Biology**C****D**



1
2
3 **Determination of the subcellular localization and mechanism of action of**
4
5 **ferrostatins in suppressing ferroptosis**
6

7 Michael M. Gaschler,^a Fanghao Hu,^a Huizhong Feng,^b Andreas Linkermann,^c Wei
8 Min,^{a, §} Brent R. Stockwell^{a,b,§}
9

10
11
12 ^a Department of Chemistry, Columbia University, New York, NY 10027
13

14 ^b Department of Biological Sciences, Columbia University, New York, NY 10027
15

16
17 ^c Medical Clinic III, Division of Nephrology, Carl Gustav Carus University Hospital
18 at the Technical University Dresden, Dresden 01309, Germany
19

20
21 [§] Co-corresponding authors: wm2256@columbia.edu, bstockwell@columbia.edu
22
23
24
25
26
27
28
29
30
31
32
33
34
35
36
37
38
39
40
41
42
43
44
45
46
47
48
49
50
51
52
53
54
55
56
57
58
59
60

Abstract

Ferroptosis is a form of non-apoptotic cell death characterized by the unchecked accumulation of lipid peroxides. Ferrostatin-1 and its analogs (ferrostatins) specifically prevent ferroptosis in multiple contexts, but many aspects of their molecular mechanism of action remain poorly described. Here, we employed stimulated Raman scattering (SRS) microscopy coupled with small vibrational tags to image the distribution of ferrostatins in cells, and found that they accumulate in lysosomes, mitochondria, and endoplasmic reticulum. We then evaluated the functional relevance of lysosomes and mitochondria to ferroptosis suppression by ferrostatins, and found that neither is required for effective ferroptosis suppression.

Introduction

Preventing cell death may be an effective strategy for treating degenerative diseases and injury. Although cell death can occur in an unregulated manner during classic necrosis, or accidental cell death, such death is often carried out by one of several molecular programs, which are collectively referred to as regulated cell death, in that they can be modulated by pharmacological or genetic manipulation. Compounds that prevent regulated cell death can be useful in multiple contexts, making them valuable tools to treat disease and injury.

Ferrostatin-1 is a potent and selective small-molecule inhibitor of ferroptosis, a form of non-apoptotic, iron-dependent, regulated cell death involving lipid peroxidation.^{1, 2} Ferrostatin-1 and its analogs (ferrostatins) prevent ferroptosis in various models of neurodegeneration,¹⁻³ acute kidney injury,^{4, 5} intracerebral hemorrhage,⁶ and other degenerative conditions,² suggesting the potential of ferrostatins as therapeutic agents. Significant exploration of the structure-activity relationship (SAR) of ferrostatins has led to analogs with increased potency and metabolic stability;^{2, 4, 7} even so, many aspects of the mechanism of ferroptosis itself, and its suppression by ferrostatins remain to be elucidated.

The correlation between increased lipophilicity and increased potency was one of the first trends discovered in exploring the SAR of ferrostatins. Increasing the lipophilicity of the hydrocarbon moiety on either one of the arylamines led to ferrostatins with greater potency.¹ Additionally, it is worth noting that all active

1
2
3 ferrostatin analogs are reducing agents that are able to reduce the stable radical
4 DPPH.^{1, 2} Structural modifications that lack such reducing behavior prevent
5
6
7
8 compounds from suppressing ferroptosis. Together, these observations led to the
9
10 hypothesis that ferrostatins function as lipophilic antioxidants that use their large
11
12 lipophilic group to anchor into cellular membranes, where they reduce lipid
13
14 hydroperoxides, or act as radical trapping antioxidants.⁸
15
16
17
18

19 We sought to gain deeper insight into the mechanism of ferrostatins to better
20
21 understand ferroptosis and to aid in the development of new ferrostatins with
22
23 improved properties. To do so, we harnessed an emerging bio-orthogonal
24
25 imaging technique known as stimulated Raman scattering (SRS) microscopy
26
27 coupled with small vibrational tags to visualize ferrostatins in live cells. We used
28
29 an integrated strategy of exploring the structure-*distribution*-activity relationship,
30
31 by iteratively varying the structures of ferrostatin analogs and examining the
32
33 corresponding intracellular distribution and drug potency. We found that
34
35 ferrostatins accumulate in specific sub-cellular regions, including lysosomes,
36
37 mitochondria, and endoplasmic reticulum, but not the plasma membrane or
38
39 nucleus. Accumulation of ferrostatins in mitochondria and lysosomes, however,
40
41 did not contribute to ferroptosis suppression.
42
43
44
45
46
47
48
49
50

51 **Results**

52
53
54
55
56
57
58
59
60

Ferrostatins accumulate in lysosomes, mitochondria, and endoplasmic reticulum

The potency of ferrostatins has been suggested to derive from their ability to anchor in lipid membranes, thereby allowing them to reduce lipid hydroperoxides, or trap radical intermediates in lipid peroxidation.² Supporting this, the rate of radical trapping by ferrostatin-1 was enhanced 7.6-fold in liposomes relative to a nonpolar solvent.⁸ We sought to image the distribution of ferrostatins in live cells in order to determine whether they preferentially localize to subcellular locations, such as specific membrane environments.

Conventional approaches to imaging the cellular distribution of small molecules involve covalent attachment of a fluorescent dye. For a compound as small as ferrostatin-1, we were concerned that covalent attachment of a bulky fluorescent dye would significantly alter its native activity and localization due to the large size of fluorescent tags. To circumvent this, we employed the emerging stimulated Raman scattering (SRS) microscopy to visualize ferrostatin distribution in living cells. By attaching small vibrational tags only a few atoms in size with characteristic vibrational frequencies in the silent region of a typical cellular Raman spectrum, bio-orthogonal chemical imaging by SRS microscopy achieves live-cell imaging of bioactive molecules with high sensitivity and specificity in a quantitative manner.⁹ Alkynes are promising SRS vibrational tags due to their strong Raman signal, lack of chemical reactivity in cells, small size, and have been successfully used for drug imaging.¹⁰ Compared to single

1
2
3 alkyne, conjugated alkynes (e.g., a diyne) further enhance the SRS signal,
4 allowing higher detection sensitivity and lower concentrations of the probe
5 compound.^{11, 12}
6
7
8
9

10
11
12 Given these considerations, we designed and synthesized diyne ferrostatin
13 analog **2** (Figure 1A). Because of the functional tolerance of ferrostatins to
14 extensive substitution at the 4 position,² we hypothesized that incorporation of a
15 diyne moiety at this position would not significantly alter the potency of
16 compound **2** relative to the parent ferrostatin-1. To maintain the lipophilicity
17 required for anti-ferroptotic activity, the diyne moiety of **2** was capped with a
18 highly lipophilic n-butyl group. The calculated octanol/water partition coefficient
19 (cLogP) of compound **2** was 3.78, making it slightly more lipophilic than
20 ferrostatin-1 (cLogP 3.2).² To validate the potency and activity of compound **2**,
21 we treated ferroptosis-sensitive HT-1080 fibrosarcoma cells with a lethal dose of
22 the ferroptosis inducer erastin, and a serial dilution of ferrostatin-1 or compound
23 **2** (Figure 1B). We found that compound **2** suppressed ferroptosis with a potency
24 similar to ferrostatin-1, confirming that the diyne tag did not significantly affect the
25 anti-ferroptotic activity of the original compound.
26
27
28
29
30
31
32
33
34
35
36
37
38
39
40
41
42
43
44
45
46

47 Having verified the anti-ferroptotic activity of probe **2**, we aimed to image its
48 distribution in living cells. First, we confirmed that the diyne tag of probe **2** shows
49 a distinct peak at 2262 cm⁻¹ within the cell Raman-silent window (Supplemental
50 figure 1). Next, HT-1080 cells were treated with **2** and erastin simultaneously,
51
52
53
54
55
56
57
58
59
60

1
2
3 and imaged by SRS microscopy after 6 h of incubation (Figure 1C). Most
4 strikingly, **2** accumulated in large puncta throughout the cytoplasm, with lesser
5 accumulation through the remainder of the cytoplasm. Notably, no significant
6 amount of **2** was detected in the nucleus or in the plasma membrane, within the
7 limits of SRS sensitivity. To test if this pattern of accumulation was specific to
8 cells undergoing ferroptosis, we incubated HT-1080 cells with probe **2** in the
9 absence of erastin (Figure 1D). We did not observe a significant change in its
10 distribution, indicating that the pattern of ferrostatin localization does not depend
11 on whether or not ferroptosis has been initiated, as might be expected. To ensure
12 this pattern of localization was not specific to HT-1080 cells, we tested diyne **2**
13 in the immortalized pancreatic cancer line Panc-1. Similar to HT-1080 cells, Panc-1
14 cells treated with diyne ferrostatin analog **2** also showed strong accumulation in
15 puncta throughout the cytosol and little accumulation within the nucleus both in
16 the presence and absence of erastin (Supplemental figure 2).
17
18
19
20
21
22
23
24
25
26
27
28
29
30
31
32
33
34
35
36
37

38 We sought to determine if this observed distribution was due to accumulation of
39 probe **2** at specific organelles. We hypothesized that the large puncta might
40 correspond to accumulation within lysosomes. HT-1080 cells were treated with
41 probe **2** for 6 h, followed by 30 min with the lysosome-targeted fluorescent dye
42 LysoTracker, and both compounds were imaged within the same cells by
43 correlative SRS and fluorescence microscopy (Figure 1E). The LysoTracker
44 signal showed partial overlap with the large puncta from probe **2**, suggesting that
45 these sites of ferrostatin accumulation were indeed lysosomes.
46
47
48
49
50
51
52
53
54
55
56
57
58
59
60

1
2
3
4
5
6 In addition to lysosomes, the mitochondria and endoplasmic reticulum (ER) have
7
8 also been hypothesized to play roles in ferroptosis,^{1, 13} and were additional sites
9
10 of localization of probe **2**. We therefore sought to examine whether probe **2**
11
12 accumulated at either of these organelles. HT-1080 cells were treated with **2** and
13
14 both a mitochondria-specific and ER-specific fluorescent dye (Figure 1F). Though
15
16 the lower signal intensity of **2** at these sites indicated that **2** was present at lower
17
18 concentrations in both of these locations than in lysosomes, **2** showed a clear
19
20 pattern of overlap with the mitochondria-specific fluorescent dye Mito Tracker
21
22 Deep Red. Due to the diffuse nature of ER network, it was unclear if the
23
24 widespread distribution of **2** was due to specific accumulation within ER, but the
25
26 image we observed was nonetheless consistent with ER accumulation of
27
28 ferrostatins, given that it was not as diffuse at the extent of cytosol. Thus, based
29
30 on the linear concentration dependence of SRS signal, we concluded that **2**
31
32 accumulates primarily in lysosomes, with additional localization in mitochondria
33
34 and ER, but did not show detectable concentrations in the plasma membrane or
35
36 the nucleus.
37
38
39
40
41
42
43

44 **Accumulation at Lysosomes Reduces the Potency of Ferrostatins**

45
46 The role of lysosomes in ferroptosis is unclear. Earlier studies reported a burst of
47
48 reactive oxygen species (ROS) in lysosomes of cells undergoing ferroptosis,¹⁴
49
50 but lysosomal membrane permeabilization, a feature of other forms of oxidative
51
52 cell damage, was not observed in cells treated with erastin.² Additionally,
53
54
55
56
57
58
59
60

1
2
3 lysosomes store iron imported by endocytosis of transferrin, a process critical for
4 ferroptosis.¹⁵ Correspondingly, the membrane-impermeable iron chelator DFO
5 likely protects against ferroptosis by chelating iron accumulated in lysosomes *via*
6 endocytosis.¹⁶
7
8
9
10
11
12

13
14 We hypothesized that ferrostatins accumulate in lysosomes because of the
15 lysosomotropic effect.¹⁷ In their neutral form, small molecules with weakly basic
16 sites (generally aromatic or aliphatic amines) can freely diffuse through lipid
17 membranes and between cellular compartments. In acidic lysosomes (pH 4.5-
18 5.0), basic groups are protonated and unable to diffuse out because of the
19 resulting positive charge. In this way, molecules can be trapped in lysosomes,
20 even if their biological target is elsewhere in a cell.¹⁸ In support of our hypothesis,
21 we calculated the acidity of the conjugate acids of each amine on ferrostatin-1 in
22 an aqueous environment. We found that the conjugate acid of the unsubstituted
23 arylamine has a pK_a of 4.6, suggesting it can be protonated in the lysosome.
24 Given the basic aromatic amines in ferrostatins and the observed high levels of
25 accumulation of probe **2** within lysosomes, we examined whether lysosomal
26 accumulation of ferrostatins was critical to their mechanism of ferroptosis rescue
27 or if lysosomotropism prevents ferrostatins from reaching their necessary targets.
28
29
30
31
32
33
34
35
36
37
38
39
40
41
42
43
44
45
46
47
48

49 We first incubated HT-1080 cells with a lethal dose of erastin and a serial dilution
50 of ferrostatin-1, as well as 0 (vehicle only), 5, or 10 μM chloroquine (Figure 2A).
51 Chloroquine is a classic lysosomotropic agent, and is protonated in lysosomes,
52
53
54
55
56
57
58
59
60

1
2
3 thus raising lysosomal pH, reducing the extent of molecular trapping by the
4 lysosomotropic effect for other compounds. We found that co-treatment of cells
5 with ferrostatin-1 and chloroquine caused an increase in the potency (lower EC₅₀)
6 of ferrostatin-1 in a chloroquine dose-dependent manner (Figure 2A).
7
8
9

10
11
12
13
14 Since preventing ferrostatin accumulation in lysosomes increased ferrostatin
15 potency (Figure 2A), we hypothesized that promoting ferrostatin accumulation in
16 lysosomes would correspondingly decrease their potency (*i.e.*, require a higher
17 concentration of ferrostatin to suppress ferroptosis). We designed and
18 synthesized ferrostatins **3** and **4**, which each contain a basic morpholine group, a
19 moiety commonly used to target molecules to lysosomes (Figure 2B)¹⁹.
20
21
22
23
24
25
26
27
28
29
30
31
32
33
34
35
36
37
38
39
40
41
42
43
44
45
46
47
48
49
50
51
52
53
54
55
56
57
58
59
60
Ferrostatin **4** has a cLogP of 1.94, slightly less lipophilic than ferrostatin-1 and
ferrostatin **2**, while ferrostatin **3** was more lipophilic with a cLogP value of 2.07.
Though such physiochemical changes might change many properties of a
compound (e.g. increased non-specific protein binding), we hypothesized that
changes in the potency of compounds **3** and **4** would mainly arise from the
protonation of the morpholine nitrogen in the lysosome, thereby increasing the
amount of ferrostatin sequestration in this organelle. Indeed, both ferrostatins **3**
and **4** showed an eight-fold loss in potency in their ability to rescue cells from
erastin-induced ferroptosis (Figure 2C), relative to ferrostatin-1. In addition, co-
treatment of cells with LysoTracker dye and either **2** or **4** revealed that, as
designed, ferrostatin **4** accumulates strongly in lysosomal compartments (Figure
2D), confirming that the decrease in potency is correlated with increased

1
2
3 sequestration in lysosomes. Cumulatively, these data suggest that reducing the
4 basicity of the ferrostatin amines could improve potency by reducing lysosomal
5 sequestration, although a careful balance between basicity and reduction
6 potential of amines needs to be considered for developing more effective
7 ferroptosis inhibitors. With the ability to perform direct SRS imaging of drug
8 distribution inside cells, this methodology is an example of exploring the
9 structure-*distribution*-activity relationship, and correlating this with the structure-
10 activity relationship.
11
12
13
14
15
16
17
18
19
20
21
22

23 **Mitochondria are not required for ferroptosis or ferroptosis rescue by** 24 **ferrostatin-1**

25
26
27
28 Since ferrostatin analog **2** showed accumulation in mitochondria, we sought to
29 determine whether mitochondria are necessary for ferroptosis, as well as for
30 ferroptosis rescue by ferrostatins. ROS generated by the mitochondrial electron
31 transport chain do not contribute to ferroptosis, as cells lacking mitochondrial
32 DNA are still sensitive to ferroptosis.¹ Still, ACSL4-dependent alterations in
33 mitochondrial morphology are observed in cells undergoing ferroptosis,^{1, 20, 21} and
34 the nitroxide antioxidant XJB-5-131, which is targeted to mitochondria, is a more
35 potent inhibitor of ferroptosis than untargeted analogs.²²
36
37
38
39
40
41
42
43
44
45
46
47
48

49 To examine the necessity of mitochondria for ferroptosis, we generated
50 mitochondria-deficient cells, using a previously reported mitophagy protocol.²³
51
52
53
54 The E3 ligase parkin causes the elimination of mitochondria lacking a membrane
55
56
57
58
59
60

1
2
3 potential *via* mitophagy, a macroautophagic process specific to mitochondria.^{23, 24}
4
5 We generated stably transfected HT-1080 cells expressing YFP-parkin or
6
7 mCherry-parkin (Figure 3A). Loss of membrane potential was induced by
8
9 treatment with the uncoupling agent carbonyl cyanide *m*-chlorophenyl hydrazine
10
11 (CCCP). Following treatment of YFP-parkin-expressing cells or mCherry-parkin-
12
13 expressing cells with CCCP for 48 h, we examined the levels of the mitochondria
14
15 specific proteins tom20 and cytochrome C (Figure 3B). Parkin-expressing cells
16
17 had highly diminished levels of both proteins after 48 hours of CCCP treatment,
18
19 confirming the elimination of most mitochondria. Extensive mitochondrial
20
21 depletion within 48 h has been observed in other cell types using this
22
23 approach.^{23, 24} We also observed near-complete absence of the complex 1 genes
24
25 Mt-Nd1 and Mt-Nd2 following CCCP treatment (Figure 3C and 3D). YFP-parkin
26
27 CCCP-treated cells also showed a decrease in immunofluorescence signal when
28
29 imaged for mitochondria-specific proteins COX IV and HSP60, while wild-type
30
31 cells showed no significant change (supplemental figure 3A). Electron
32
33 microscopy imaging of YFP-parkin-expressing cells treated with CCCP confirmed
34
35 a significant decrease in the number of observable mitochondria by TEM (Figure
36
37 3E and supplemental figure 3B). YPF-parkin cells depleted of mitochondria also
38
39 showed a large increase in the abundance of endoplasmic reticulum and/or Golgi
40
41 bodies (supplemental figure 3B). Cells depleted of mitochondria showed a greatly
42
43 decreased growth rate, but were nonetheless persistent in cell culture over
44
45 multiple days.
46
47
48
49
50
51
52
53
54
55
56
57
58
59
60

1
2
3 To examine the necessity of mitochondria for ferroptosis, we treated YFP-Parkin-
4 expressing HT-1080 cells with a panel of ferroptosis-inducing compounds. All
5 ferroptosis inducers tested effectively killed cells depleted of mitochondria in a
6 similar oxidative, dose-dependent manner to cells harboring mitochondria (Figure
7 3F, Supplemental figure 3C, and Supplemental figure 4), indicating that the
8 presence of mitochondria is not necessary for ferroptosis. Staurosporine, an
9 inducer of mitochondria-dependent apoptosis, caused no loss in viability over all
10 concentrations tested, confirming that mitochondria had been effectively and
11 functionally removed, and that staurosporine-induced apoptosis requires
12 mitochondria, as expected. Notably, inhibitors of system x_c^- (erastin and IKE)
13 both became somewhat less potent following CCCP treatment (i.e. after
14 mitophagy), while RSL3 and FIN56, which target GPX4, both became somewhat
15 more potent after mitophagy. When CCCP was withdrawn at the time of
16 ferroptosis induction, these potency shifts for FIN56 and RSL3 did not change
17 significantly, confirming that these changes in potency were the direct result of
18 mitophagy and not an off-target effect of the presence of CCCP (supplemental
19 figure 3C). The level of GPX4 protein, a master regulator of ferroptosis, did not
20 decrease in mitochondria-depleted HT-1080 cells relative to wildtype HT-1080
21 cells treated with CCCP (supplemental figure 3D). Additionally, wild-type HT-
22 1080 cells treated with CCCP were still sensitive to staurosporine and showed no
23 change in sensitivity to ferroptosis inducers, other than the modest resistance to
24 system x_c^- inhibitors noted above (supplemental figure 3E).
25
26
27
28
29
30
31
32
33
34
35
36
37
38
39
40
41
42
43
44
45
46
47
48
49
50
51
52
53
54
55
56
57
58
59
60

1
2
3 We then evaluated the ability of ferroptosis-suppressing compounds to prevent
4 ferroptosis in cells depleted of mitochondria. Both ferrostatin-1 and iron chelators
5 (deferroxamine and ciclopirox olamine) were able to prevent erastin-induced
6 ferroptosis in a dose-dependent manner (supplemental figure 3F and 3G),
7 confirming that the mechanism of erastin lethality was consistent with ferroptosis
8 in CCCP-treated YFP-parkin cells. We evaluated the potency of ferrostatin-1 in
9 YFP-parkin-transfected HT-1080 cells following mitophagy (Figure 3G). Cells
10 were treated with a lethal concentration of either the class 1 ferroptosis inducer
11 erastin or the class 2 ferroptosis inducer RSL3,¹⁶ and a serial dilution of
12 ferrostatin-1. In both cases, ferrostatin-1 became moderately more potent
13 following mitophagy, indicating that mitochondria are not required for ferroptosis
14 suppression by ferrostatins.
15
16
17
18
19
20
21
22
23
24
25
26
27
28
29
30
31
32

33 The data above suggest that mitochondria are not necessary for ferroptosis
34 induction and neither mitochondria nor lysosomes are necessary for ferroptosis
35 induction or ferrostatin action, despite the prominent accumulation of ferrostatin-1
36 in these organelles. Together with the overall distribution of diene ferrostatin **2**
37 observed by SRS (Figure 1C), this suggests that the location in which ferrostatin
38 exerts its anti-ferroptotic action is likely the ER, unless there is another relevant
39 location with very low levels of ferrostatin present, below the detection limit of
40 SRS. The hypothesis that ER is the site of ferrostatin action is supported by the
41 increased potency of ferrostatin-1 in post-mitophagy cells, which showed greater
42 ER abundance (supplemental figure 3B).
43
44
45
46
47
48
49
50
51
52
53
54
55
56
57
58
59
60

Discussion

In this study, we sought to gain insight into the mechanism of ferroptosis suppression by ferrostatin-1. The ability of ferrostatin-1 to act as a reducing agent was one of the earliest observed properties of the compound,¹ and served as the basis for initial hypotheses about its mechanism of action.²

We sought to understand where ferrostatin-1 accumulates inside cells, as enrichment within a ferroptosis-relevant organelle could explain the high potency of Fer-1. By employing SRS microscopy coupled with small vibrational tags, we observed significant localization of ferrostatins within lysosomes, mitochondria, and the endoplasmic reticulum, and minimal accumulation within the nucleus and plasma membrane. We hypothesized that, as the nexus of iron import and trafficking, lysosomes might play a critical role in ferroptosis. Instead we found that accumulation within lysosomes actually decreased the overall potency of ferrostatins, while preventing ferrostatin accumulation in lysosomes by chloroquine treatment increased ferrostatin-1 potency.

To examine the role of ferrostatin localization at mitochondria, we generated a stably transfected cell line that was depleted of mitochondria. We found that mitochondria-deficient cells were still sensitive to ferroptosis, and could still be rescued by ferrostatins and iron chelators. It should be noted that a very small number of mitochondria may still remain in these cells, and we cannot yet rule

1
2
3 out a role for such a residual population of mitochondria in initiating a chain
4 reaction of lipid peroxidation; nonetheless, we can state that mitochondria are not
5 the primary site of lipid peroxidation during ferroptosis. By varying the structures
6 of ferrostatin analogues, examining the corresponding intracellular distribution
7 and drug potency, and using this information to guide iterative rounds of structure
8 design, we are adopting a strategy of integrating the structure-distribution-activity
9 relationship. Such a methodology can be applied to study the mechanism of
10 other drugs.
11
12
13
14
15
16
17
18
19
20
21
22
23

24 Together, these data suggest that ferrostatin accumulation within the
25 endoplasmic reticulum could be critical to ferroptosis suppression, and that the
26 ER may also be critical to ferroptosis initiation. The ER lumen is an oxidative
27 environment and might initiate ferroptosis as a consequence of ER-related
28 oxidative stress. Alternately, the ER is the source of lipids for most membranes in
29 other organelles and contains more than half of all lipid bilayers in any given
30 cell.²⁵ Therefore, it is possible that ferrostatin accumulation within the ER is the
31 most efficient strategy to maintain overall peroxide tone within cellular
32 membranes; ER localization would allow ferrostatins to prevent oxidation of the
33 majority of cellular lipids, thereby decreasing lipid peroxide abundance.
34
35
36
37
38
39
40
41
42
43
44
45
46
47
48

49 **Methods**

50
51 **Cell lines and media.** HT-1080 cells were obtained from ATCC and grown in
52 DMEM with glutamine and sodium pyruvate (Corning 10-013) supplemented with
53
54
55
56
57
58
59
60

1
2
3 10% Heat-Inactivated FBS, 1% non-essential amino acids (Invitrogen), and 1%
4 penicillin-streptomycin mix (Invitrogen). Panc-1 cells were obtained from ATCC
5 and grown in DMEM with glutamine and sodium pyruvate (Corning 10-013)
6 supplemented with 10% Heat-Inactivated FBS, and 1% penicillin-streptomycin
7 mix (Invitrogen). Phoenix-AMPHO (ATCC: CRL-3213) were grown in DMEM
8 supplemented with 10% heat-inactivated FBS, 1% penicillin-streptomycin mix
9 (Invitrogen), and 2 mM L-glutamine. All cells were maintained in a humidified
10 environment at 37 °C and 5% CO₂ in a tissue incubator.
11
12
13
14
15
16
17
18
19
20
21
22

23
24 **Ferroptosis rescue assay.** 3,000 cells were seeded per well in black, clear
25 bottom 384-well plates (Corning) and allowed to adhere overnight. The next day,
26 the medium was replaced with 50 µL of growth medium and 5 µL medium
27 containing erastin (10 µM) or (1S, 3R)-RSL3 (2 µM) and a dilution series of the
28 ferroptosis-suppressing compound. 24 h later, 6.1 µL of Presto Blue (Thermo-
29 Fisher) was added. Cells were incubated for an additional 5 h, and the Presto
30 Blue fluorescence intensity was measured using a Victor X5 plate reader
31 (PerkinElmer)(ex/em 530/590). Background (no cells) fluorescence was
32 subtracted and the resulting fluorescence intensities were averaged between
33 biological replicates. From these data, dose-response curves and EC₅₀ values
34 were computed using Prism 7.0 (GraphPad). For mitophagy experiments, YFP-
35 Parkin transfected HT-1080 cells were cultured in medium containing 12.5 µM
36 CCCP for 24 h. Cells were then trypsinized, suspended and seeded into white,
37 opaque-bottom 384-well plates (Corning) at a density of 3,000 cells per well in 50
38
39
40
41
42
43
44
45
46
47
48
49
50
51
52
53
54
55
56
57
58
59
60

1
2
3 μL medium containing 12.5 μM CCCP and allowed to adhere for 24 additional
4
5 hours (48 h CCCP treatment in total). The medium was either kept or replaced
6
7 with CCCP-free medium (herein designated "+CCCP" or "+Mitophagy -CCCP",
8
9 respectively), and treated with 5 μL medium containing molecules as described
10
11 above. Viability was assayed using CellTiter-Glo® (Promega) according to the
12
13 manufacturer's protocol. Luminescence was read on a Victor X5 plate reader and
14
15 data were analyzed as described above.
16
17
18
19
20

21 **Computational methods:** Computational determination of octanol/water
22
23 partition coefficient (ClogP) was performed in MOE 2016.0802 using the Slog P
24
25 function (Chemical Computing Group). Compound pKa was calculated using
26
27 Jaguar pKa (Schrödinger Inc.)
28
29

30 **SRS microscopy.** An integrated laser source (picoEMERALD, Applied Physics
31
32 & Electronics, Inc.), is used to produce both a Stokes beam (1064 nm, 6 ps,
33
34 intensity modulated at 8 MHz) and a tunable pump beam (720 to 990 nm, 5–6
35
36 ps) at 80 MHz repetition rate. Two spatially and temporally overlapped beams
37
38 are coupled into an inverted multiphoton laser-scanning microscope
39
40 (FV1200MPE, Olympus) with optimized near-IR throughput. Both beams are
41
42 focused on the cell samples through either a 25 \times water objective (XLPlan N, 1.05
43
44 N.A. MP, Olympus) or a 60 \times water objective (UPlanAPO/IR, 1.2 N.A., Olympus),
45
46 and collected with an high N.A. oil condenser lens (1.4 N.A., Olympus) after the
47
48 sample. By blocking the Stokes beam with a high O.D. bandpass filter (890/220
49
50 CARS, Chroma Technology), only the pump beam is collected with a large area
51
52
53
54
55
56
57
58
59
60

1
2
3 Si photodiode (FDS1010, Thorlabs) reverse-biased by 64 DC voltage. The output
4 current of photodiode is filtered electronically (KR 2724, KR electronics),
5 terminated with 50 Ω , and demodulated with a RF lock-in amplifier (SR844,
6 Stanford Research Systems) with near shot-noise-limited sensitivity. The
7 stimulated Raman loss signal at each pixel is sent to the analog interface box
8 (FV10-ANALOG, Olympus) of the microscope to generate the image. All images
9 (512 \times 512 pixels) are acquired with 30 μ s time constant at the lock-in amplifier
10 and 100 μ s pixel dwell time (\sim 27 s per frame). Measured after the objectives, 12
11 mW pump power and 40 mW Stokes power are used to image the 2940 cm^{-1}
12 channel. 48 or 88 mW pump beam and 120 mW Stokes beam are used to image
13 the 2262 cm^{-1} and 2000 cm^{-1} channels.
14
15
16
17
18
19
20
21
22
23
24
25
26
27
28
29
30

31 **Spontaneous Raman spectroscopy.** Raman spectra are collected on a
32 confocal Raman microscope (Xplora, Horiba Jobin Yvon with LabSpec 6
33 software) at room temperature. The sample is excited through a 50 \times air
34 objective (MPlan N, 0.75 N.A., Olympus) with a 532-nm diode laser (27 mW after
35 the objective). The acquisition time for ferrostatin 2 in DMSO solution was 20 s.
36
37
38
39
40
41
42
43
44

45 **Sample preparation for SRS and fluorescence imaging of live cells.** HT-
46 1080 and Panc-1 cells are seeded on glass coverslips in 4-well plates with \sim 1 mL
47 of culture media one day before experiment. After the treatment, cells are
48 washed with phosphate buffered saline (PBS, Sigma) for 3 times and the
49 coverslip with cells is assembled into a chamber filled with PBS solution for
50
51
52
53
54
55
56
57
58
59
60

1
2
3 imaging. Fluorescence imaging is performed using the Olympus FV1200 confocal
4 microscope with standard laser excitation and bandpass filter set for each dye.
5
6 All images are assigned color and analyzed by ImageJ.
7
8
9

10
11
12 **Cell Transfection** Phoenix-AMPHO (ATCC: CRL-3213) cells were seeded in a
13 6-well plate at 800,000 cells/well. After 20 h, the medium was changed to 800 μ L
14 Opti-mem in each well. A solution of Lipofectamine 2000 (6 μ L) in 100 μ L Opti-
15 mem media (reduced serum media) and YFP-Parkin-IRES-zeocin (Addgene,
16 #61728) plasmid (2.5 μ g) or mCherry-Parkin-IRES-zeocin (Addgene, #61727)
17 plasmid (2.5 μ g) each in 100 μ L Opti-mem media were combined and incubated
18 20 min at room temperature, then added to each well. After 4 h, 1 mL Opti-mem
19 with 20% FBS was added to each well. 24 h later, the medium was replaced with
20 10% FBS, 1% penicillin-streptomycin mix (Invitrogen), 2 mM L-glutamine in
21 DMEM. The next day the supernatant was collected three times spaced 4 h apart
22 and polybrene was added (1:1000 dilution). The supernatant was filtered (0.45
23 μ m filters) and added to HT1080 cells seeded at 160,000 cells per well (6-well
24 dish) in 2 mL portions spaced 4 h apart. After 48 h, the cells were trypsinized and
25 re-seeded in medium containing zeocin (400 μ g/mL). After 2 weeks of selection
26 with zeocin, the HT1080 cells were then used in subsequent assays, and
27 cultured in standard HT-1080 medium.
28
29
30
31
32
33
34
35
36
37
38
39
40
41
42
43
44
45
46
47
48
49
50

51 **Western blotting** Cells were seeded in growth medium and left untreated or
52 treated with 12.5 μ M CCCP, after 24 h the medium was washed out and replaced
53
54
55
56
57
58
59
60

1
2
3 with fresh medium containing 12.5 μ M CCCP and incubated 24 h more (48 h
4 total). Medium was then aspirated from each dish and cells washed twice with
5 cold PBS. Cells were lysed in 60 μ L RIPA buffer with protease inhibitors. Unlysed
6 cells and debris were pelleted for 15 min at 16,000 xg at 4°C. Samples were
7 separated using SDS-PAGE and transferred to nitrocellulose membranes.
8 Transfer was performed using the iBlot system (Invitrogen). Membranes were
9 treated with Li-COR Odyssey blocking buffer for 1 h at room temperature, then
10 incubated with primary antibody in a 1:1 solution of PBS-T and Li-COR odyssey
11 blocking buffer overnight at 4°C. Following three 5 min washes in PBS-T, the
12 membrane was incubated with secondary antibodies (1:3000) in a 1:1 solution of
13 PBS-T and Li-COR Odyssey blocking buffer for 1 h at room temperature.
14 Following three 5 min washes in PBS-T, membranes were scanned using the Li-
15 COR Odyssey Imaging System. Antibodies for cytochrome c (BD Biosciences),
16 tom20 (Santa Cruz) and parkin (Sigma-Aldrich) were detected using a goat anti-
17 rabbit or goat anti-mouse IgG antibody conjugated to an IRdye at 800CW and
18 680CW conjugated, respectively (Li-COR Biosciences).
19
20
21
22
23
24
25
26
27
28
29
30
31
32
33
34
35
36
37
38
39
40
41

42 **Quantitative PCR (qPCR)** Cells with and without CCCP treatment were
43 detached from 100 mm culture dishes, and 3 million cells were collected as a
44 pellet by centrifuging 1,000 rpm for 5 min. Total cellular DNA sample was
45 prepared using DNeasy Blood & Tissue Kit (QIAGEN) according to
46 manufacturer's instruction. Primers for qPCR were designed with NCBI Primer-
47 BLAST. qPCR was performed using Power SYBR Green Master Mix (Applied
48
49
50
51
52
53
54
55
56
57
58
59
60

1
2
3 Biosystems) in a 96-well format, in triplicate, using viiA7 Real-Time PCR system
4
5 (Life Technologies). Comparative analysis ($\Delta\Delta C_t$ analysis) was performed with
6
7 Pecam and 18s as internal reference genes.
8
9

10
11
12 **Immunofluorescence** Cells with and without CCCP treatment were fixed with
13
14 4% formaldehyde for 20 minutes at room temperature. Following fixation, cells
15
16 were permeabilized in PBS-T buffer (0.1% Triton in PBS) for 10 min and blocked
17
18 in blocking buffer (5% normal goat serum in PBT) for 1 hour at room
19
20 temperature. Cells were incubated overnight at 4°C with anti-COX IV antibody
21
22 (Abcam) and anti-HSP60 antibody (Abcam) 1/1000 diluted in blocking buffer.
23
24 Cells were washed three 5 min in PBS-T (0.05% Tween20 in PBS) then
25
26 incubated with goat anti-mouse IgG antibody conjugated to an IRdye at 680CW
27
28 (Li-COR Biosciences) for 1 h at room temperature. Cells were washed three 5
29
30 min in PBS-T and mounted on slides with ProLong™ Diamond Antifade
31
32 Mountant with DAPI (Thermo Fisher). Slides were analyzed using Zeiss LSM 700
33
34 confocal microscope. Fluorescence intensities were quantified with Image J
35
36 software.
37
38
39
40
41
42
43

44
45 **Electron microscopy** Fixed cells were incubated with 2.5% glutaraldehyde and
46
47 2% paraformaldehyde in 100 mM cacodylate buffer (pH 7.4) overnight. Samples
48
49 were then treated with 1% osmium tetroxide in 100 mM cacodylate buffer for 1 h,
50
51 washed in distilled water four times (10 min/wash), and then treated with 1–2%
52
53 aqueous uranyl acetate overnight at 4°C in the dark. Samples were then washed
54
55
56
57
58
59
60

1
2
3 and sequentially dehydrated with increasing concentrations of acetone (20, 30,
4 50, 70, 90, and 100%) for 30 min each, followed by three additional treatments
5 with 100% acetone for 20 min each. Samples were then infiltrated with increasing
6 concentrations of Spurr's resin (25% for 1 h, 50% for 1 h, 75% for 1 h, 100% for 1
7 h, 100% overnight at room temperature), and then incubated overnight at 70°C in
8 a resin mold. Sections of 50–90 nm were cut on a Leica ultramicrotome with a
9 diamond knife. Imaging then took place using an FEI Talos F200X operating at
10 200kV.
11
12
13
14
15
16
17
18
19
20
21
22

23 **Acknowledgements**

24 M. Gaschler was supported by the NIH Training Program in Molecular Biophysics
25 Grant T32GM008281. B. Stockwell was supported by NIH/NCI (R35CA209896
26 and P01CA087497). W. Min acknowledges support from the NIH Director's New
27 Innovator Award, NIH R01 (Grant EB020892), the Alfred P. Sloan Foundation
28 and the Camille and Henry Dreyfus Foundation. Electron microscopy studies
29 were performed by C. Goulbourne. We would like to acknowledge Columbia
30 University's Nanoscience Initiative for the use of its shared facilities, and the Fu
31 Foundation School of Engineering and Applied Science and the Faculty of Arts &
32 Sciences for their support of the CNI Facilities.
33
34
35
36
37
38
39
40
41
42
43
44
45
46
47
48

49 **Author Contributions**

50 M.M.G., F.H, W.M., B.R.S., contributed to the writing of the manuscript; all
51 authors have given their approval of the final version of the manuscript. M.M.G.,
52
53
54
55
56
57
58
59
60

1
2
3 F.H., A.L., B.R.S., and W.M. designed research. M.M.G., F.H., H.F., performed
4
5 research.
6
7
8
9

10 Supporting Information

11
12 Supporting information, consisting of additional methods and four figures, is
13
14 available free of charge via the internet at <http://pubs.acs.org>.
15
16
17
18

19 References

- 20
21
22 1. Dixon, S. J., Lemberg, K. M., Lamprecht, M. R., Skouta, R., Zaitsev, E. M., Gleason, C.
23 E., Patel, D. N., Bauer, A. J., Cantley, A. M., Yang, W. S., Morrison, B., 3rd, and
24 Stockwell, B. R. (2012) Ferroptosis: an iron-dependent form of nonapoptotic
25 cell death, *Cell* *149*, 1060-1072.
- 26
27 2. Skouta, R., Dixon, S. J., Wang, J., Dunn, D. E., Orman, M., Shimada, K., Rosenberg, P.
28 A., Lo, D. C., Weinberg, J. M., Linkermann, A., and Stockwell, B. R. (2014)
29 Ferrostatins inhibit oxidative lipid damage and cell death in diverse disease
30 models, *J Am Chem Soc* *136*, 4551-4556.
- 31
32 3. Kabiraj, P., Valenzuela, C. A., Marin, J. E., Ramirez, D. A., Mendez, L., Hwang, M. S.,
33 Varela-Ramirez, A., Fenelon, K., Narayan, M., and Skouta, R. (2015) The
34 neuroprotective role of ferrostatin-1 under rotenone-induced oxidative
35 stress in dopaminergic neuroblastoma cells, *Protein J* *34*, 349-358.
- 36
37 4. Linkermann, A., Skouta, R., Himmerkus, N., Mulay, S. R., Dewitz, C., De Zen, F.,
38 Prokai, A., Zuchtriegel, G., Krombach, F., Welz, P. S., Weinlich, R., Vanden
39 Berghe, T., Vandenabeele, P., Pasparakis, M., Bleich, M., Weinberg, J. M.,
40 Reichel, C. A., Brasen, J. H., Kunzendorf, U., Anders, H. J., Stockwell, B. R.,
41 Green, D. R., and Krautwald, S. (2014) Synchronized renal tubular cell death
42 involves ferroptosis, *Proc Natl Acad Sci U S A* *111*, 16836-16841.
- 43
44 5. Martin-Sanchez, D., Ruiz-Andres, O., Poveda, J., Carrasco, S., Cannata-Ortiz, P.,
45 Sanchez-Nino, M. D., Ruiz Ortega, M., Egido, J., Linkermann, A., Ortiz, A., and
46 Sanz, A. B. (2017) Ferroptosis, but Not Necroptosis, Is Important in
47 Nephrotoxic Folic Acid-Induced AKI, *J Am Soc Nephrol* *28*, 218-229.
- 48
49 6. Li, Q., Han, X., Lan, X., Gao, Y., Wan, J., Durham, F., Cheng, T., Yang, J., Wang, Z., Jiang,
50 C., Ying, M., Koehler, R. C., Stockwell, B. R., and Wang, J. (2017) Inhibition of
51 neuronal ferroptosis protects hemorrhagic brain, *JCI Insight* *2*, e90777.
- 52
53 7. Hofmans, S., Vanden Berghe, T., Devisscher, L., Hassannia, B., Lyssens, S., Joossens,
54 J., Van Der Veken, P., Vandenabeele, P., and Augustyns, K. (2016) Novel
55 Ferroptosis Inhibitors with Improved Potency and ADME Properties, *J Med*
56
57
58
59
60 *Chem* *59*, 2041-2053.

- 1
2
3 8. Zilka, O., Shah, R., Li, B., Friedmann Angeli, J. P., Griesser, M., Conrad, M., and Pratt,
4 D. A. (2017) On the Mechanism of Cytoprotection by Ferrostatin-1 and
5 Liproxstatin-1 and the Role of Lipid Peroxidation in Ferroptotic Cell Death,
6 *ACS Cent Sci* 3, 232-243.
- 7
8 9. Wei, L., Hu, F., Chen, Z., Shen, Y., Zhang, L., and Min, W. (2016) Live-Cell
9 Bioorthogonal Chemical Imaging: Stimulated Raman Scattering Microscopy
10 of Vibrational Probes, *Acc Chem Res* 49, 1494-1502.
- 11
12 10. Wei, L., Hu, F., Shen, Y., Chen, Z., Yu, Y., Lin, C. C., Wang, M. C., and Min, W. (2014)
13 Live-cell imaging of alkyne-tagged small biomolecules by stimulated Raman
14 scattering, *Nat Methods* 11, 410-412.
- 15
16 11. Yamakoshi, H., Dodo, K., Palonpon, A., Ando, J., Fujita, K., Kawata, S., and Sodeoka,
17 M. (2012) Alkyne-tag Raman imaging for visualization of mobile small
18 molecules in live cells, *J Am Chem Soc* 134, 20681-20689.
- 19
20 12. Lee, H. J., Zhang, W., Zhang, D., Yang, Y., Liu, B., Barker, E. L., Buhman, K. K.,
21 Slipchenko, L. V., Dai, M., and Cheng, J. X. (2015) Assessing cholesterol storage
22 in live cells and *C. elegans* by stimulated Raman scattering imaging of phenyl-
23 Diyne cholesterol, *Sci Rep* 5, 7930.
- 24
25 13. Dixon, S. J., Patel, D. N., Welsch, M., Skouta, R., Lee, E. D., Hayano, M., Thomas, A.
26 G., Gleason, C. E., Tatonetti, N. P., Slusher, B. S., and Stockwell, B. R. (2014)
27 Pharmacological inhibition of cystine-glutamate exchange induces
28 endoplasmic reticulum stress and ferroptosis, *Elife* 3, e02523.
- 29
30 14. Torii, S., Shintoku, R., Kubota, C., Yaegashi, M., Torii, R., Sasaki, M., Suzuki, T.,
31 Mori, M., Yoshimoto, Y., Takeuchi, T., and Yamada, K. (2016) An essential role
32 for functional lysosomes in ferroptosis of cancer cells, *Biochem J* 473, 769-
33 777.
- 34
35 15. Gao, M., Monian, P., Quadri, N., Ramasamy, R., and Jiang, X. (2015) Glutaminolysis
36 and Transferrin Regulate Ferroptosis, *Mol Cell* 59, 298-308.
- 37
38 16. Cao, J. Y., and Dixon, S. J. (2016) Mechanisms of ferroptosis, *Cell Mol Life Sci* 73,
39 2195-2209.
- 40
41 17. Deduve, C., Debarsy, T., Poole, B., Trouet, A., Tulkens, P., and Vanhoof, F. (1974)
42 Lysosomotropic Agents, *Biochem Pharmacol* 23, 2495-&.
- 43
44 18. Fu, D., Zhou, J., Zhu, W. S., Manley, P. W., Wang, Y. K., Hood, T., Wylie, A., and Xie,
45 X. S. (2014) Imaging the intracellular distribution of tyrosine kinase
46 inhibitors in living cells with quantitative hyperspectral stimulated Raman
47 scattering, *Nat Chem* 6, 614-622.
- 48
49 19. Dong, B., Song, X., Wang, C., Kong, X., Tang, Y., and Lin, W. (2016) Dual Site-
50 Controlled and Lysosome-Targeted Intramolecular Charge Transfer-
51 Photoinduced Electron Transfer-Fluorescence Resonance Energy Transfer
52 Fluorescent Probe for Monitoring pH Changes in Living Cells, *Anal Chem* 88,
53 4085-4091.
- 54
55 20. Friedmann Angeli, J. P., Schneider, M., Proneth, B., Tyurina, Y. Y., Tyurin, V. A.,
56 Hammond, V. J., Herbach, N., Aichler, M., Walch, A., Eggenhofer, E.,
57 Basavarajappa, D., Radmark, O., Kobayashi, S., Seibt, T., Beck, H., Neff, F.,
58 Esposito, I., Wanke, R., Forster, H., Yefremova, O., Heinrichmeyer, M.,
59 Bornkamm, G. W., Geissler, E. K., Thomas, S. B., Stockwell, B. R., O'Donnell, V.
60 B., Kagan, V. E., Schick, J. A., and Conrad, M. (2014) Inactivation of the

- ferroptosis regulator Gpx4 triggers acute renal failure in mice, *Nat Cell Biol* **16**, 1180-1191.
21. Doll, S., Proneth, B., Tyurina, Y. Y., Panzilius, E., Kobayashi, S., Ingold, I., Irmeler, M., Beckers, J., Aichler, M., Walch, A., Prokisch, H., Trumbach, D., Mao, G., Qu, F., Bayir, H., Fullekrug, J., Scheel, C. H., Wurst, W., Schick, J. A., Kagan, V. E., Angeli, J. P., and Conrad, M. (2017) ACSL4 dictates ferroptosis sensitivity by shaping cellular lipid composition, *Nat Chem Biol* **13**, 91-98.
22. Krainz, T., Gaschler, M. M., Lim, C., Sacher, J. R., Stockwell, B. R., and Wipf, P. (2016) A Mitochondrial-Targeted Nitroxide Is a Potent Inhibitor of Ferroptosis, *ACS Cent Sci* **2**, 653-659.
23. Tait, S. W., Oberst, A., Quarato, G., Milasta, S., Haller, M., Wang, R., Karvela, M., Ichim, G., Yatim, N., Albert, M. L., Kidd, G., Wakefield, R., Frase, S., Krautwald, S., Linkermann, A., and Green, D. R. (2013) Widespread mitochondrial depletion via mitophagy does not compromise necroptosis, *Cell Rep* **5**, 878-885.
24. Narendra, D., Tanaka, A., Suen, D. F., and Youle, R. J. (2008) Parkin is recruited selectively to impaired mitochondria and promotes their autophagy, *J Cell Biol* **183**, 795-803.
25. Alberts, B. (2002) *Molecular biology of the cell*, 4th ed., Garland Science, New York.
26. Yang, W. S., SriRamaratnam, R., Welsch, M. E., Shimada, K., Skouta, R., Viswanathan, V. S., Cheah, J. H., Clemons, P. A., Shamji, A. F., Clish, C. B., Brown, L. M., Girotti, A. W., Cornish, V. W., Schreiber, S. L., and Stockwell, B. R. (2014) Regulation of ferroptotic cancer cell death by GPX4, *Cell* **156**, 317-331.

Figure legends

Figure 1. SRS imaging of ferrostatins in live HT-1080 cells. (A) Structure of ferrostatin-1 (**1**) and diyne ferrostatin (**2**). (B) Potency of ferrostatin analogs in HT-1080 cells treated with erastin (10 μ M). Viability was measured 24 h after treatment. (C) SRS images of ferrostatin **2** (10 μ M) in live HT-1080 cells treated with erastin (10 μ M). Images gathered 6 h after compound addition. (D) SRS image of ferrostatin **2** (10 μ M) in live HT-1080 cells in the absence of erastin. Images gathered 6 h after compound addition. (E) Co-localization of signal from live HT-1080 cells treated with erastin and ferrostatin **2** (10 μ M each) for 6 h and

1
2
3 Lyso Tracker Red (100 nM) for 30 min. (F) SRS or fluorescence signal from live
4 HT-1080 cells treated with erastin and ferrostatin **2** (10 μ M each) for 6 h and
5 MitoTracker Deep Red (200 nM) for 30 min, or ERTracker Green (2 μ M) for 1 h.
6
7
8
9
10 Scale bars, 10 μ M.

11
12
13
14 **Figure 2.** Accumulation within lysosomes reduces ferrostatin potency. (A)
15 Decreasing EC_{50} of ferrostatin-1 mediated erastin (10 μ M) rescue in the
16 presence of 0, 5, and 10 μ M chloroquine. Viability was measured at 24 h after
17 compound treatment. Column height represents EC_{50} value with error bars
18 corresponding to the 95% confidence interval. (B) Structure of lysosome-targeted
19 ferrostatin **3** and SRS-compatible lysosome targeted ferrostatin **4**. (C) Potency of
20 ferrostatins in suppressing ferroptosis initiated by erastin (10 μ M). (D) Signal in
21 live HT-1080 cells treated with erastin and ferrostatins **2** or **4** (10 μ M each, 6 h)
22 and LysoTracker Red (100 nM, 30 min). Scale bars, 10 μ M.

23
24
25
26
27
28
29
30
31
32
33
34
35
36
37
38 **Figure 3.** Cells depleted of mitochondria are still sensitive to ferroptosis inducers
39 and ferrostatins. (A) Western blot of parkin protein levels in wild type and
40 transfected HT-1080 cells in the presence and absence of CCCP. (B) Western
41 blot of tom20 and cytochrome C proteins in wild type, YFP-parkin, and mCherry-
42 parkin transfected HT-1080 cells following treatment with CCCP (12.5 μ M) for 48
43 h. (C and D) Nd1 mRNA abundance (C) and Nd2 mRNA abundance (D) in wild
44 type and transfected cells in the presence or absence of CCCP (12.5 μ M for 48
45 h). (E) Quantification of mitochondria abundance from electron microscopy
46
47
48
49
50
51
52
53
54
55
56
57
58
59
60

1
2
3 images in wild type and YFP-parkin transfected HT-1080 cells in the absence
4 and presence of CCCP (12.5 μ M for 48 h). (F) Potency of ferroptosis inducers
5 and the apoptosis inducer staurosporine in YFP-parkin expressing HT-1080 cells
6 with (-CCCP) and without (+CCCP) mitochondria. Column height represents
7 EC_{50} value with error bars corresponding to the 95% confidence interval. (G)
8 Potency of ferrostatin-1 in preventing erastin or RSL3 initiated ferroptosis in YFP-
9 parkin expressing HT-1080 cells with (-CCCP) and without (+CCCP)
10 mitochondria. Column height represents EC_{50} value with error bars
11 corresponding to the 95% confidence interval.
12
13
14
15
16
17
18
19
20
21
22
23
24
25
26
27
28
29
30
31
32
33
34
35
36
37
38
39
40
41
42
43
44
45
46
47
48
49
50
51
52
53
54
55
56
57
58
59
60

